Intersite Coulomb Repulsion Driven Quadrupole Instability and Magnetic Ordering in the Orbital Frustrated Ba_2MgReO_6

Xuanye Zhang[1†], Jinyu Zou[1†], and Gang Xu[1,2,3*]

[1] *Wuhan National High Magnetic Field Center & School of Physics, Huazhong University of Science and Technology, Wuhan 430074, China*
[2] *Institute for Quantum Science and Engineering, Huazhong University of Science and Technology, Wuhan 430074, China*
[3] *Wuhan Institute of Quantum Technology, Wuhan 430074, China*

(Received 13 May 2025; accepted manuscript online 19 May 2025)

In order to calculate the multipoles in real materials with considerable intersite Coulomb interaction V, we develop a self-consistent program which starts from the first-principles calculations to solve the tight-binding Hamiltonian including onsite Coulomb repulsion U, V, and spin-orbital coupling λ. The program is applied to Ba_2MgReO_6 to figure out the mechanism of structural instability and magnetic ordering. A comprehensive quadrupole phase diagram versus U and V with $\lambda = 0.28$ eV is calculated. Our results demonstrate that the easy-plane anisotropy and the intersite Coulomb repulsion V must be considered to remove the orbital frustration. The increase of V to > 20 meV would arrange quadrupole $Q_{x^2-y^2}$ antiparallelly, accompanied by small parallel $Q_{3z^2-r^2}$, and stabilize Ba_2MgReO_6 into the body-centered tetragonal structure. Such antiparallel $Q_{x^2-y^2}$ provides a new mechanism for the Dzyaloshinskii–Moriya interaction and gives rise to the canted antiferromagnetic (CAF) state along the [110] axis. Moreover, sizable octupoles such as O_{21}^{31}, O_{21}^{33}, O_{21}^{34} and O_{21}^{36} are discovered for the first time in the CAF state. Our study not only provides a comprehensive understanding of the experimental results in Ba_2MgReO_6, but also serves as a general and useful tool for the study of multipole physics in 5d compounds.

DOI: 10.1088/0256-307X/42/7/070703 CSTR: 32039.14.0256-307X.42.7.070703

1. Introduction. Usually, there are two remarkable characteristics of 5d electrons. One is the dramatically enhanced spin-orbital coupling (SOC) λ, which originates from the large atomic number Z. The other is the spatially extended orbital, which could lead to considerable intersite Coulomb repulsion V. In the past decades, the interplay between onsite Coulomb repulsion U and SOC with comparable energy, and the resulting exotic properties in 5d transition metal (TM) compounds, have attracted increasing interest, including the SOC assistant Mott metal–insulator transition,[1–3] non-collinear magnetic moment,[4–7] orbital frustration,[8–10] and high-rank multipoles.[11–16] Among them, the orbital-frustrated honeycomb and face-centered cubic (FCC) lattice magnets have been extensively studied recently, which are reported to host the long-pursuit quantum spin liquid states when the orbital frustration is maintained and dominates,[17–19] or give rise to lattice distortion accompanied by orbital ordering when orbital frustration is eliminated.[20–23] However, while most efforts have been focused on the interplay between U and λ and the resulting properties,[24–31] rare works pay attention to the influence of V, though it could play a key role to determine the exotic states and properties in 5d TM compounds. Especially in the field of first-principles calculations, a general program to handle U, V, and λ self-consistently is still lacking.

The double perovskite Ba_2MgReO_6 with $5d^1$ configuration, adopting the frustrated FCC lattice, provides an ideal platform to study the interplay between U, λ, and V, as well as the resulting exotic properties.[32–42] Ba_2MgReO_6 undergoes two phase transitions upon cooling, including FCC to BCT (body-centered tetragonal) phase transition at T_q and canted antiferromagnetic (CAF) phase transition with a small gap at T_m.[35,36,38,42] Further synchrotron X-ray diffraction measurements of high-quality single crystals show that the tetragonal distortion is enhanced below T_m, indicating the coupling between quadrupoles and magnetic orders.[36] Recently, the magnetic entropy was obtained by subtracting the phonon contribution from heat capacity,[42] which reflects the $N = 2$ degeneracy of the ground state multipoles, in contrast to Ref. [35]. These evidences imply that the pure spin model is not enough to describe the magnetic mechanism in Ba_2MgReO_6. In fact, strong SOC not only leads to small magnetic dipole ordering, as small as $0.3\,\mu_B$ in Ba_2MgReO_6, but also opens up the possibility of high-rank multipoles.[14,43] Such high-rank multipoles are usually entangled with the magnetic dipole ordering, making them difficult to detect through conventional experiments.[12,13] Therefore, a comprehensive understanding of the phase

†These authors contributed equally to this work.
*Corresponding author. Email: gangxu@hust.edu.cn
© 2025 Chinese Physical Society and IOP Publishing Ltd. All rights, including for text and data mining, AI training, and similar technologies, are reserved.

transitions and exotic properties in Ba_2MgReO_6 remains elusive until now.

The previous microscopic model studies involving V have reported the rich multipole ordering states.[40,43] These model studies mainly focus on the 16 multipoles $O^K_{\Gamma\lambda}$, which are only applicable to the $J_{\rm eff} = 3/2$ subspace in the strong SOC limit, whereas the SOC in real 5d compounds is not strong enough to separate $J_{\rm eff} = 3/2$ and $J_{\rm eff} = 1/2$ subspaces, necessitating the complete 36 multipoles $O^{KM}_{K_1K_2}$.[14] In this paper, to calculate all the possible multipole orders in a real material, we start from the first-principles calculations and construct the tight-binding Hamiltonian including U, λ, and especially V to develop a self-consistent program. This program figures out the influence of V on the multipoles in real materials, thereby uncovering the nature of phase transition and exotic properties. In Ba_2MgReO_6, our calculation demonstrates that, while the easy-plane anisotropy can partially remove the orbital frustration, the intersite Coulomb repulsion V is indispensable to fully remove the frustration and generate the right orbital ordering to meet the experiment. The calculations reveal that the antiparallel (AP) $Q_{x^2-y^2}$ predominantly minimizes the intersite Coulomb repulsion energy. Hence, a small $V = 20$ meV is sufficient to stabilize Ba_2MgReO_6 into the BCT structure, accompanied by the AP-$Q_{x^2-y^2}$ and a small parallel $Q_{3z^2-r^2}$ quadrupole component. Such a quadrupole state with incompletely quenched orbital angular momentum provides a new mechanism of Dzyaloshinskii–Moriya (DM) interaction, explaining the experimentally observed CAF ground state.[35,36] Moreover, various magnetic octupoles are discovered in the CAF ground state, where the octupoles have comparable magnitudes with magnetic dipoles and also exhibit a canted arrangement along the [110] direction. This complex magnetic structure likely explains the anomalous magnetic entropy and weak magnetic anisotropy in the CAF ground state.

2. Calculation Methods. As shown in Fig. 1(a), Ba_2MgReO_6 adopts a double perovskite structure with the $Fm\bar{3}m$ space group.[35,37] The crystal field of the local oxygen octahedron splits the d-orbitals of the Re atom into higher doubly-degenerate e_g orbitals and lower triply-degenerate t_{2g} orbitals.[44,45] With a $5d^1$ configuration, the t_{2g} orbitals are sufficient to describe the low-energy physics of Ba_2MgReO_6. The one-electron occupation usually leads to spontaneous symmetry breaking with orbital ordering,[46–51] which can be expanded by the quadrupole orders $Q_{x^2-y^2}$ (abbreviated as Q_{x^2}) and $Q_{3z^2-r^2}$ (abbreviated as Q_{z^2}),

$$\begin{aligned} Q_{x^2} &= \frac{1}{2}(n_{xz} - n_{yz})\,, \\ Q_{z^2} &= \frac{\sqrt{3}}{6}(n_{xz} + n_{yz} - 2n_{xy})\,, \end{aligned} \tag{1}$$

where n_α ($\alpha = xy, xz, yz$) is electron occupation. The Q_{x^2} breaks O_h to D_{2h} and Q_{z^2} breaks O_h to D_{4h}, corresponding to the octahedral distortion shown in Figs. 1(b) and 1(c) respectively.

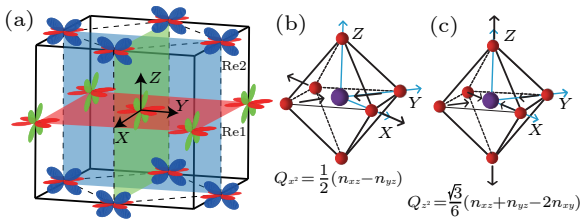

Fig. 1. (a) Schematic of Re1 and Re2 atoms in FCC unit cell (solid line) and BCT structure (dashed lines). XY, XZ and YZ planes (orbitals) are indicated by red, green, and blue colors. (b) and (c) The oxygen octahedral distortion modes corresponding to Q_{x^2} and Q_{z^2} orders.

In order to comprehensively investigate the effects of intersite Coulomb repulsion V on the orbital ordering and physical properties in Ba_2MgReO_6, we base our study on the DFT+U+V method[52,53] to develop a self-consistent calculation package to calculate the 36 multipole orders of real materials. The full Hamiltonian $H = H_{\rm tb}+H_{\rm SOC}+H_U+H_V$ is constructed from the density functional theory (DFT)-calculated tight-binding Hamiltonian with the addition of the Coulomb interaction terms H_U and H_V, and is solved by self-consistently calculating the multipole orders, as shown in Fig. 2. Starting from the FCC structure with a lattice constant $a = 8.0802$ Å,[36] the tight-binding Hamiltonian $H_{\rm tb}$ is obtained by constructing the maximally localized Wannier function of t_{2g} using the Vienna *ab initio* simulation[54,55] and WANNIER90 package.[56–58] The spin-orbit coupling $H_{\rm SOC}$ adopts the form of $\lambda \boldsymbol{S}\cdot\boldsymbol{L}_{t_{2g}}$, with the spin and effective orbital angular momentum $S = \frac{1}{2}$ and $L_{t_{2g}} = 1$. $\lambda = 0.28$ eV is determined by fitting the non-magnetic (NM) band structures.

The onsite interaction H_U adopts the form of Kanamori Hamiltonian,

$$H_U = (U-3J)\frac{\hat{N}(\hat{N}-1)}{2} - 2J\boldsymbol{S}^2 - \frac{J}{2}\boldsymbol{L}^2 + \frac{5}{2}J\hat{N}, \tag{2}$$

with the occupation number $\hat{N} = \sum_{i,\alpha} n_{i,\alpha}$ and Hund's coupling $J/U = 0.1$. Applying the mean field approximation, the correlation interaction can be solved directly by the unrestricted Hartree–Fock method,

$$\begin{aligned} c^\dagger_\alpha c^\dagger_\beta c_\delta c_\gamma \approx\ & \rho_{\beta\delta}c^\dagger_\alpha c_\gamma + \rho_{\alpha\gamma}c^\dagger_\beta c_\delta - \rho_{\beta\delta}\rho_{\alpha\gamma} \\ & - \rho_{\beta\gamma}c^\dagger_\alpha c_\delta - \rho_{\alpha\delta}c^\dagger_\beta c_\gamma + \rho_{\beta\gamma}\rho_{\alpha\delta}, \end{aligned} \tag{3}$$

where $\rho_{\alpha\beta} = \langle c^\dagger_\alpha c_\beta\rangle$ is the local density matrix.[59] One may worry about the double counting of U in the DFT+U calculation. Notice that our self-consistent calculations focus on the t_{2g} orbitals without the d–p Coulomb interaction. Thus, the double counting term is just a constant for specific U and can be absorbed into the chemical potential.[14,16] When we compare the total energy between different ordering states at the same U, the double counting term is the same constant due to the same local occupation number, which is 1 for the $5d^1$ configuration in Ba_2MgReO_6. Therefore, the double counting will not cause any problem in our calculations.

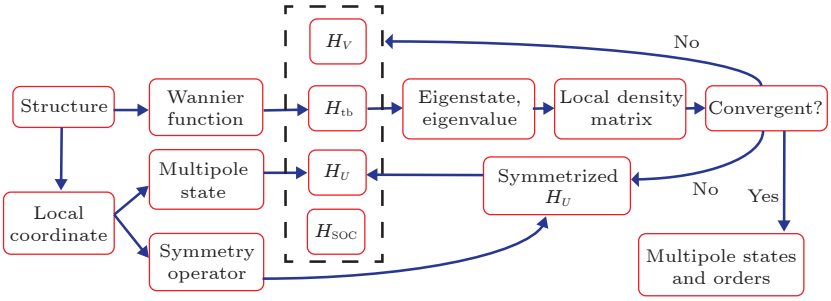

Fig. 2. The flow chart to calculate the multipole orders based on the first-principles calculations.

The intersite repulsion of t_{2g} is $H_V = \sum_{\langle i,j\rangle} \cdot V_{ij}^{\alpha\beta} n_{i,\alpha} n_{j,\beta}$. According to the electric quadrupole approximation,[43] $V_{ij}^{\alpha\beta}$ can be reduced to a single variable V. Considering the d^1 configuration and ignoring the constant, it becomes

$$H_V = V \sum_{\alpha} \sum_{\langle i,j\rangle \in \alpha} \left[\frac{4}{3}(n_{i,\beta} - n_{i,\gamma}) \times (n_{j,\gamma} - n_{j,\beta}) + \frac{4}{9} n_{i,\alpha} n_{j,\alpha} \right], \quad (4)$$

in which $\alpha \neq \beta \neq \gamma$ and $\langle i,j\rangle \in \alpha$ denote that the bond between i and j is in the plane of α orbital. With the Hartree approximation, H_V is solved as

$$H_V = V \sum_{\alpha} \sum_{\langle i,j\rangle \in \alpha} \left[\frac{4}{3}(\overline{n}_{j,\gamma} - \overline{n}_{j,\beta}) \times \left(n_{i,\beta} - \frac{\overline{n}_{i,\beta}}{2} - n_{i,\gamma} + \frac{\overline{n}_{i,\gamma}}{2} \right) + \frac{4}{9} \left(\overline{n}_{j,\alpha} n_{i,\alpha} - \frac{\overline{n}_{j,\alpha} \overline{n}_{i,\alpha}}{2} \right) + (i \leftrightarrow j) \right], \quad (5)$$

where $\overline{n} = \langle n \rangle$ can be obtained directly from the local density matrix.

To release the orbital frustration of cubic symmetry, our calculation is performed in the BCT structure, as illustrated by the dashed line in Fig. 1(a). This superstructure has the same lattice as the cubic but with the vector $Q = 2\pi(001)$, which has been widely reported in double perovskite materials.[60–64] The flow of the calculation program has been plotted in Fig. 2. For the reason that H_V is obtained by local density matrix, the Hamiltonian in the first loop only contains H_{tb}, H_{SOC}, and H_U, where H_U is expressed in terms of all the multipole order parameters.[16] To perform the self-consistent calculation, the initial trial state is chosen according to the symmetry requirements. In the NM calculations, all the possible initial states with the combination of quadrupoles allowed by the symmetries are considered. In the magnetic calculations, all the symmetry-allowed possible trial states with dipole and octupole orders are considered. The constructed Hamiltonian is then diagonalized to calculate the local density matrix and further obtain the order parameters as well as the expression of H_V for the next loop. The energy accuracy used for our calculation is set as 10^{-6} eV.

3. Results of Quadrupole. We first perform the NM calculation to study the quadrupole orders. Figure 3(a) displays the phase diagram as a function of U and V. The order is absent in the small U regime (phase I), while it emerges at large U (phase II with quadrupole orders $\pm\mu Q_{x^2} - \nu Q_{z^2}$ and phase III with quadrupole order (AP-Q_{x^2})+Q_{z^2}, see details below). This result agrees with reports that the onsite Coulomb repulsion U is the driving force of the orbital ordering in many materials.[65–71]

Dashed lines in Fig. 3(b) compare the energy of quadrupole orders as a function of U with $V = 0$, which finds that doubly-degenerate orders $+\mu Q_{x^2} - \nu Q_{z^2}$ and $-\mu Q_{x^2} - \nu Q_{z^2}$ ($\mu \neq \frac{\sqrt{3}}{2}$ and $\nu \neq \frac{1}{2}$) become the most stable states when $U > 1.2$ eV (phase II). Such orders reflect that the electron in Ba_2MgReO_6 tends to occupy d_{xy} orbital, which implies the easy-plane anisotropy, as also mentioned in previous work.[43] The doubly degeneracy means the partial breaking of orbital frustration in phase II; however, this is insufficient to interpret the nondegenerate quadrupole order in experiments.[36]

However, the introduction of V can drive the material into phase III and give rise to the experimentally reported AP quadrupole order,[36] as shown in Fig. 3(c), which demonstrates that the AP-Q_{x^2} combined with a small parallel Q_{z^2} order [abbreviated as (AP-Q_{x^2})+Q_{z^2}] replaces $\pm\mu Q_{x^2} - \nu Q_{z^2}$ to become the ground state when $V > 20$ meV. Such order would lead to the occupation as sketched in Fig. 1(a), which shows that electrons on the Re1/Re2 atoms prefer more d_{xz}/d_{yz} orbitals and less d_{xy}, so that the energy caused by V would be efficiently reduced by keeping the eletrons on Re1 and Re2 away from each other. Such a mechanism is confirmed by the increment of the alternative occupation of d_{xz} and d_{yz} orbitals on Re1 and Re2 and the reduction of the d_{xy} with the increasing of V, giving rise to the increment/reduction of AP-Q_{x^2} order/Q_{z^2} order, as demonstrated by the red lines in Fig. 3(d).

All these results demonstrate that the intersite Coulomb repulsion V is the key factor for 5d compounds to obtain the right order, and such order is stable against the increase of U, as shown by the solid lines in Fig. 3(b), which present the energy evolution of different orders and clearly demonstrate that (AP-Q_{x^2})+Q_{z^2} order is stabilized when $U > 1$ eV and its energy advantage grows with the increase of U.

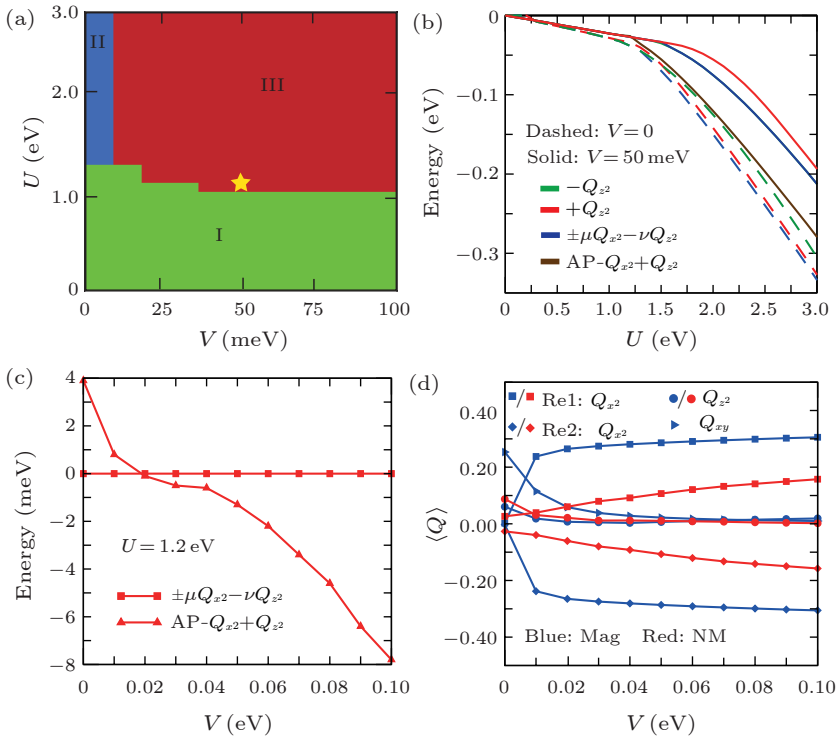

Fig. 3. (a) The quadrupole phase diagram versus U and V. The SOC strength is $\lambda = 0.28$ eV, and Hound's coupling is taken as $J/U = 0.1$. Regions I, II, and III represent cubic, $\pm\mu Q_{x^2} - \nu Q_{z^2}$, and (AP-$Q_{x^2}$)+$Q_{z^2}$ states, respectively. Ba_2MgReO_6 is located at the position marked by the yellow star. (b) The total energy of ordering states depending on U with $V = 0$ (dashed lines) and $V = 50$ meV (solid lines). (c) The energy difference between $\pm\mu Q_{x^2} - \nu Q_{z^2}$ and (AP-Q_{x^2})+Q_{z^2} states with the increasing of V. (d) Evolution of quadrupole orders in (AP-Q_{x^2})+Q_{z^2} state with V increasing. Red and blue lines represent the NM and CAF magnetic states, respectively. U is set as 1.2 eV in (c) and (d).

4. Results of Magnetic Order. In the following, we perform the calculation with the breaking of time-reversal symmetry to clarify that (AP-Q_{x^2})+Q_{z^2} order would give rise to the experimentally reported CAF configuration. From the AP-Q_{x^2} order and the expression $Q_{x^2} = \frac{1}{2}(L_x^2 - L_y^2)$ with $L_x = \mathrm{i}d_{xz}^\dagger d_{xy} + \text{h.c.}$ and $L_y = \mathrm{i}d_{xy}^\dagger d_{yz} + \text{h.c.}$,[14] one can notice that the L_x and L_y on two Re atoms are exchanged ($L_{x,y}$ of Re1 $\leftrightarrow$ $L_{y,x}$ of Re2) and connected by a glide mirror symmetry $\{M_{110}|(0, a/2, a/2)\}$ as demonstrated in Fig. 4(a). Thus, the angular momenta form a canted angle, which provides a new mechanism of DM interaction $\sum_{\langle i,j\rangle} D_z(\boldsymbol{S}_i \times \boldsymbol{S}_j)$ in spin space,[72–74] as SOC is considered. Such DM interaction is an intrinsic property of orbital frustration and would induce the CAF along the [110] easy-axis, as confirmed by the self-consistent magnetic calculations in Fig. 4(b), which demonstrate that the ground CAF state is about 75 meV lower than the other magnetic configurations.

The results of the CAF state reproduce the experimentally observed dipole and quadrupole orders well. The ratio between $L_x + 2S_x$ ($0.296\mu_B$) and $L_y + 2S_y$ ($0.128\mu_B$) of Re1 is approximately 2.3, leading to a $0.322\mu_B$ magnetic moment with a canted angle $\phi \sim 22°$ along the [110] direction, which agrees with $0.3\mu_B$ and $\phi \sim 40°$ in experiments.[36] Moreover, the CAF state displays an obviously enhanced Q_{x^2} order compared to that of the NM state, as shown in Fig. (d), which coincides well with the experimental report about quadrupole increment below T_m.[36]

In Fig. 4(c) with $U = 1.1$ eV, $\lambda = 0.28$ eV, and $V = 50$ meV, the band structures of the CAF ground state give rise to a Mott insulating state and a band gap of about 0.33 eV, which agrees with the experimental observation (0.17 eV).[35] The projection in Fig. 4(c) also demonstrates that the occupied bands have more $|J_{\text{eff}} = 3/2, m = \pm 1/2\rangle$ (red) components than $|J_{\text{eff}} = 3/2, m = \pm 3/2\rangle$ (blue), which agrees with the (AP-Q_{x^2})+Q_{z^2} order. We use these fitting parameters to determine the position of Ba_2MgReO_6 in the quadrupole phase diagram, as shown by the yellow star in Fig. (a), which is close to the phase boundary between phase III and phase I. This result gives a possible explanation for the quadrupole vanishing and magnetic phase transition under pressure in Ba_2MgReO_6.[39]

Furthermore, our calculations uncover that the CAF state of Ba_2MgReO_6 also has considerable octupoles including O_{21}^{31}, O_{21}^{33}, O_{21}^{34}, and O_{21}^{36}. We plot the evolution of octupoles on Re1 with the increase of U in Fig. 4(d), which illustrates the emergence and stabilization of the octupoles when $U > 0.5$ eV. According to the symmetry of these octupoles,[14] the $\{M_{110}|(0, a/2, a/2)\}$ operation of the AP-Q_{x^2} state enforces the relationship of the octupoles on the two Re atoms as $O_{21}^{31}(\text{Re2}) = O_{21}^{34}(\text{Re1})$ and $O_{21}^{33}(\text{Re1}) = -O_{21}^{36}(\text{Re2})$, as listed in Table 1. Therefore, the AP-Q_{x^2} state makes octupoles also have a canted ordering. Since the magnitude of octupoles is as large as

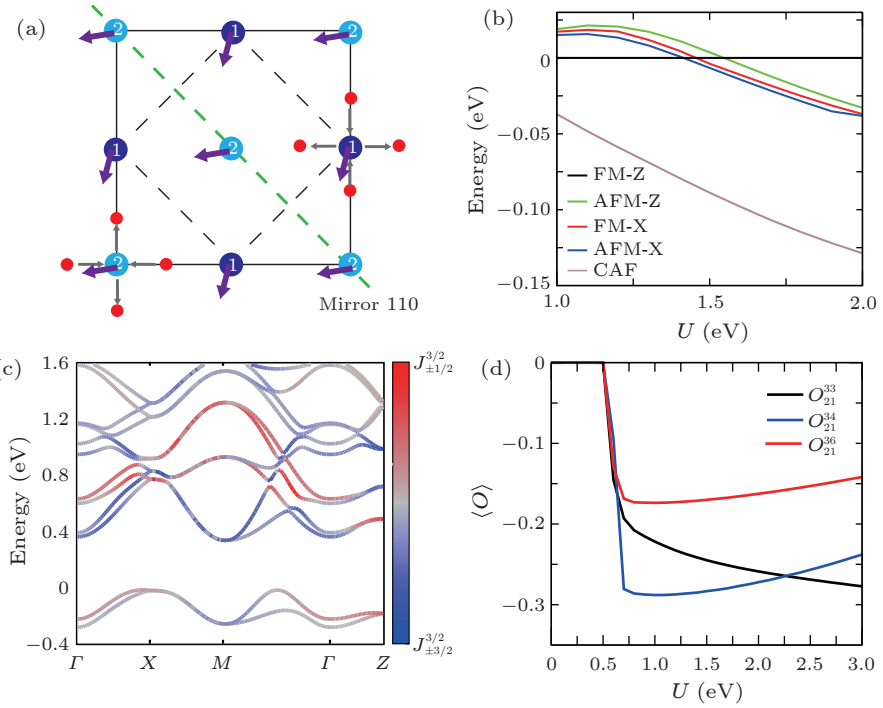

Fig. 4. (a) The schematic illustration of the glide mirror symmetry $\{M_{110}|(0, a/2, a/2)\}$ and the CAF magnetic configuration. From the top view of the lattice, the Re1 and Re2 atoms are labeled as 1 and 2. The red small balls represent the oxygen atoms, with the thin arrows representing the distortion of the octahedra corresponding to the AP-Q_{x^2} order. The green dashed line illustrates the plane of the mirror reflection M_{110}. The thick violet arrows illustrate the magnetic moment on Re atoms respecting $\{M_{110}|(0, a/2, a/2)\}$ symmetry. (b) Total energy of magnetic states relative to FM-Z with the increasing of U, where FM-Z (X) and AFM-Z (X) represent the ferromagnetic and antiferromagnetic states with the moment along z (x) direction, respectively. (c) Band structures of the CAF ground state at $U = 1.1$ eV. (d) The magnitude of Re1's octupoles in the CAF ground state depending on U, including O_{21}^{33}, O_{21}^{34}, and O_{21}^{36}. All the calculations are performed with $V = 50$ meV.

Table 1. The magnitude of magnetic octupoles at $\lambda = 0.28$ eV, $U = 1.1$ eV, and $V = 50$ meV in the CAF ground state.

	O_{21}^{31}	O_{21}^{33}	O_{21}^{34}	O_{21}^{36}
Re1	0.0051	−0.2276	−0.2880	−0.1735
Re2	−0.2880	0.1735	0.0051	0.2276

dipoles, they should have a significant influence on the responses to the external field. It would be interesting and important to detect and control such canted octupoles in the future study of Ba_2MgReO_6.

5. Conclusion. In summary, we consider the intersite Coulomb interaction V in the self-consistent calculations to calculate the complete 36 multipoles $O_{K_1K_2}^{KM}$ for the first time to investigate the phase transition mechanism and ground state properties in Ba_2MgReO_6. The orbital frustration of the cubic structure can be partially lifted by the anisotropy and further fully lifted by V. Our calculations demonstrate that $\pm\mu Q_{x^2} - \nu Q_{z^2}$ states are 8 meV lower than the Q_{z^2} state in the BCT structure, suggesting the native easy-plane anisotropy favors d_{xy} occupation. In contrast to the easy-plane anisotropy, V suppresses d_{xy} occupation and leads to the alternative majority of d_{yz} and d_{xz} orbitals along the [001] direction. As a result, the system is stabilized in the (AP-Q_{x^2})+Q_{z^2} quadrupole state when V is larger than 20 meV. We uncover that this AP-Q_{x^2} ordering can induce DM interaction between Re1 and Re2 and finally results in the CAF ground state along the [110] direction, in excellent agreement with experimental observations. Besides, our calculations discover the additional octupoles O_{21}^{31}, O_{21}^{33}, O_{21}^{34}, and O_{21}^{36} in the CAF state, which also present a canted angle with considerable magnitude. These results establish a profound understanding of the relationship between interactions, structural instability, magnetic properties, and octupoles in Ba_2MgReO_6. The program developed in this work provides a generic powerful first-principles tool for accurate investigation of other 5d TM compounds.

Aknowlegements. The authors thank Xi Dai, Yilin Wang, Zhida Song, Jianzhou Zhao, Wenxuan Qiu and Aiyun Luo for valuable discussion. This work was supported by the National Key Research and Development Program of China (Grant Nos. 2024YFA1611200 and 2018YFA0307000), and the National Natural Science Foundation of China (Grant Nos. 12274154 and 12404182).

References

[1] Kim B J, Jin H, Moon S J, Kim J Y, Park B G, Leem C S, Yu J, Noh T W, Kim C, Oh S J, Park J H, Durairaj V, Cao G, and Rotenberg E 2008 *Phys. Rev. Lett.* **101** 076402

[2] Kim B J, Ohsumi H, Komesu T, Sakai S, Morita T, Takagi H, and Arima T 2009 *Science* **323** 1329

[3] Jeong J, Lenz B, Gukasov A, Fabrèges X, Sazonov A, Hutanu V, Louat A, Bounoua D, Martins C, Biermann S,

Brouet V, Sidis Y, and Bourges P 2020 *Phys. Rev. Lett.* **125** 097202
[4] Disseler S M, Dhital C, Amato A, Giblin S R, de la Cruz C, Wilson S D, and Graf M J 2012 *Phys. Rev. B* **86** 014428
[5] Witczak-Krempa W and Kim Y B 2012 *Phys. Rev. B* **85** 045124
[6] Shinaoka H, Hoshino S, Troyer M, and Werner P 2015 *Phys. Rev. Lett.* **115** 156401
[7] Lu L, Song M, Liu W, Reyes A, Kuhns P, Lee H, Fisher I, and Mitrović V 2017 *Nat. Commu.* **8** 14407
[8] Wu C 2008 *Phys. Rev. Lett.* **100** 200406
[9] Mostovoy M V and Khomskii D I 2002 *Phys. Rev. Lett.* **89** 227203
[10] Khaliullin G, Churchill D, Stavropoulos P P, and Kee H Y 2021 *Phys. Rev. Res.* **3** 033163
[11] Witczak-Krempa W, Chen G, Kim Y B, and Balents L 2014 *Annu. Rev. Condens. Matter Phys.* **5** 57
[12] Zhao L, Torchinsky D, Chu H, Ivanov V, Lifshitz R, Flint R, Qi T, Cao G, and Hsieh D 2016 *Nat. Phys.* **12** 32
[13] Liang T, Hsieh T H, Ishikawa J J, Nakatsuji S, Fu L, and Ong N P 2017 *Nat. Phys.* **13** 599
[14] Wang Y, Weng H, Fu L, and Dai X 2017 *Phys. Rev. Lett.* **119** 187203
[15] Maharaj D D, Sala G, Stone M B, Kermarrec E, Ritter C, Fauth F, Marjerrison C A, Greedan J E, Paramekanti A, and Gaulin B D 2020 *Phys. Rev. Lett.* **124** 087206
[16] Qiu W X, Zou J Y, Luo A Y, Cui Z H, Song Z D, Gao J H, Wang Y L, and Xu G 2021 *Phys. Rev. Lett.* **127** 147202
[17] Balents L 2010 *Nature* **464** 199
[18] Chaloupka J c v, Jackeli G, and Khaliullin G 2010 *Phys. Rev. Lett.* **105** 027204
[19] Yamaji Y, Nomura Y, Kurita M, Arita R, and Imada M 2014 *Phys. Rev. Lett.* **113** 107201
[20] Oikawa K, Kamiyama T, Kato H, and Tokura Y 2003 *J. Phys. Soc. Jpn.* **72** 1411
[21] Khomskii D and Mostovoy M 2003 *J. Phys. A* **36** 9197
[22] Yuan B, Clancy J P, Sears J A, Kolesnikov A I, Stone M B, Yamani Z, Won C, Hur N, Jeon B C, Noh T W, Paramekanti A, and Kim Y J 2018 *Phys. Rev. B* **98** 214433
[23] Cong R, Nanguneri R, Rubenstein B, and Mitrović V F 2019 *Phys. Rev. B* **100** 245141
[24] Xiang H J and Whangbo M H 2007 *Phys. Rev. B* **75** 052407
[25] Yang B J and Kim Y B 2010 *Phys. Rev. B* **82** 085111
[26] Moon E G, Xu C, Kim Y B, and Balents L 2013 *Phys. Rev. Lett.* **111** 206401
[27] Schaffer R, Lee E K H, Yang B J, and Kim Y B 2016 *Rep. Prog. Phys.* **79** 094504
[28] Cong R, Nanguneri R, Rubenstein B, and Mitrović V 2020 *J. Phys. Condens. Matter* **32** 405802
[29] Ishikawa H, Takayama T, Kremer R K, Nuss J, Dinnebier R, Kitagawa K, Ishii K, and Takagi H 2019 *Phys. Rev. B* **100** 045142
[30] da Cruz Pinha Barbosa V, Xiong J, Tran P M *et al.* 2022 *Chem. Mate.* **34** 1098
[31] Mansouri Tehrani A, Soh J R, Pásztorová J, Merkel M E, Živković I, Rønnow H M, and Spaldin N A 2023 *Phys. Rev. Res.* **5** L012010
[32] Bramnik K G, Ehrenberg H, Dehn J K, and Fuess H 2003 *Solid State Sci.* **5** 235
[33] Marjerrison C A, Thompson C M, Sala G *et al.* 2016 *Inorg. Chem.* **55** 10701
[34] Dar S A, Srivastava V, Sakalle U K, and Pagare G 2018 *Computational Condensed Matter* **14** 137
[35] Hirai D and Hiroi Z 2019 *J. Phys. Soc. Jpn.* **88** 064712
[36] Hirai D, Sagayama H, Gao S, Ohsumi H, Chen G, Arima T h, and Hiroi Z 2020 *Phys. Rev. Res.* **2** 022063
[37] Takayama T, Chaloupka J, Smerald A, Khaliullin G, and Takagi H 2021 *J. Phys. Soc. Jpn.* **90** 062001
[38] Lovesey S W and Khalyavin D D 2021 *Phys. Rev. B* **103** 235160
[39] Arima H, Oshita Y, Hirai D, Hiroi Z, and Matsubayashi K 2022 *J. Phys. Soc. Jpn.* **91** 013702
[40] Svoboda C, Zhang W, Randeria M, and Trivedi N 2021 *Phys. Rev. B* **104** 024437
[41] Mansouri Tehrani A and Spaldin N A 2021 *Phys. Rev. Mater.* **5** 104410
[42] Pásztorová J, Tehrani A M, Živković I, Spaldin N A, and Rønnow H M 2022 arXiv:2210.13616
[43] Chen G, Pereira R, and Balents L 2010 *Phys. Rev. B* **82** 174440
[44] Maekawa S, Tohyama T, Barnes S. E, Ishihara S, Koshibae W, and Khaliullin G 2004 *Physics of transition metal oxides*, volume 144, Springer Science & Business Media
[45] Stamokostas G L and Fiete G A 2018 *Phys. Rev. B* **97** 085150
[46] Kugel K and Khomskii D 1973 *Zh. Eksp. Teor. Fiz* **64** 1429
[47] Kugel K I and Khomski D 1982 *Soviet Physics Uspekhi* **25** 231
[48] Elfimov I S, Anisimov V I, and Sawatzky G A 1999 *Phys. Rev. Lett.* **82** 4264
[49] Suzuki T, Katsumura M, Taniguchi K, Arima T, and Katsufuji T 2007 *Phys. Rev. Lett.* **98** 127203
[50] Kargarian M, Wen J, and Fiete G A 2011 *Phys. Rev. B* **83** 165112
[51] Liu W, Cong R, Reyes A P, Fisher I R, and Mitrović V F 2018 *Phys. Rev. B* **97** 224103
[52] Jr V L C and Cococcioni M 2010 *J. Phys.: Condens. Matter* **22** 055602
[53] Tancogne-Dejean N and Rubio A 2020 *Phys. Rev. B* **102** 155117
[54] Kresse G and Furthmüller J 1996 *Phys. Rev. B* **54** 11169
[55] Kresse G and Furthmüller J 1996 *Comput. Mater. Sci.* **6** 15
[56] Mostofi A A, Yates J R, Pizzi G *et al.* 2014 *Comput. Phys. commun.* **185** 2309
[57] Mostofi A A, Yates J R, Lee Y S, Souza I, Vanderbilt D, and Marzari N 2008 *Comput. Phys. commun.* **178** 685
[58] Marzari N, Mostofi A A, Yates J R, Souza I, and Vanderbilt D 2012 *Rev. Mod. Phys.* **84** 1419
[59] Zhuang M, Zhang W, and Ming N 1998 *Phys. Rev. B* **57** 10705
[60] Stitzer K E, Smith M D, and zur Loye H C 2002 *Solid State Sci.* **4** 311
[61] Yamamura K, Wakeshima M, and Hinatsu Y 2006 *J. Solid State Chem.* **179** 605
[62] Erickson A S, Misra S, Miller G J, Gupta R R, Schlesinger Z, Harrison W A, Kim J M, and Fisher I R 2007 *Phys. Rev. Lett.* **99** 016404
[63] Morrow R, Taylor A E, Singh D, Xiong J, Rodan S, Wolter A, Wurmehl S, Büchner B, Stone M, Kolesnikov A *et al.* 2016 *Sci. Rep.* **6** 1
[64] Gao S, Hirai D, Sagayama H, Ohsumi H, Hiroi Z, and Arima T h 2020 *Phys. Rev. B* **101** 220412
[65] Jeng H T, Guo G Y, and Huang D J 2004 *Phys. Rev. Lett.* **93** 156403
[66] Jeng H T, Lin S H, and Hsue C S 2006 *Phys. Rev. Lett.* **97** 067002
[67] Jeng H T, Guo G Y, and Huang D J 2006 *Phys. Rev. B* **74** 195115
[68] Sarkar S, Maitra T, Valentí R, and Saha-Dasgupta T 2009 *Phys. Rev. Lett.* **102** 216405
[69] Gangopadhyay S and Pickett W E 2015 *Phys. Rev. B* **91** 045133.
[70] Willa K, Willa R, Welp U, Fisher I R, Rydh A, Kwok W K, and Islam Z 2019 *Phys. Rev. B* **100** 041108
[71] Gangopadhyay S and Pickett W E 2016 *Phys. Rev. B* **93** 155126
[72] Katsura H, Nagaosa N, and Balatsky A V 2005 *Phys. Rev. Lett.* **95** 057205
[73] Moriya T 1960 *Phys. Rev.* **120** 91
[74] Dzyaloshinsky I 1958 *J. Phys. Chem. Solids* **4** 241